Journal of The Electrochemical Society, **155** (3) B236-B243 (2008)
0013-4651/2008/155(3)/B236/8/$23.00 © The Electrochemical Society

Oxygen Reduction Behavior of Highly Porous Non-Noble Metal Catalysts Prepared by a Template-Assisted Synthesis Route

Arnd Garsuch,[a] Ryan d'Eon,[a] Tara Dahn,[a,*] Olaf Klepel,[b] Rita R. Garsuch,[a] and Jeffrey R. Dahn[a,*,z]

[a]*Department of Physics and Atmospheric Science, Dalhousie University, Halifax, Nova Scotia B3H 3J5, Canada*
[b]*Institut für Technische Chemie, Universität Leipzig, 04103 Leipzig, Germany*

Highly porous non-noble metal catalysts have been prepared by template-assisted synthesis, a nanocasting procedure. A mesoporous silica gel was used to prepare different oxygen reduction catalysts. The synthesis procedure consists of the following steps: impregnation of the template with different transition metal salts ($FeCl_3$ or $CoCl_2$), pore filling of the impregnated host material with pyrrole, polymerization of pyrrole with hydrochloric acid and subsequent carbonization in argon as well as final liberation of the catalyst material by dissolving the template framework and the transition metal in hydrofluoric acid. The obtained catalyst samples are highly porous and exhibit outstanding oxygen reduction behavior. The Brunauer, Emmett, and Teller method surface areas between 670 and 1030 m^2/g and pore volumes ranging from 1.6 to 2.4 cm^3/g have been observed. Onset potentials up to 0.85 V were recorded during the oxygen reduction reaction (ORR). Different parameters affecting ORR activity (e.g., metal source, metal concentration of host material, annealing temperature) have been investigated and are discussed. Corresponding non-noble metal catalysts have been characterized by X-ray diffraction measurements, elemental analysis, scanning electron microscopy, and nitrogen adsorption.
 [DOI: 10.1149/1.2825168]

Manuscript submitted October 1, 2007; revised manuscript received November 7, 2007. Available electronically January 11, 2008.

The preparation of porous carbons by template-assisted synthesis routes has been developed in order to obtain materials with high surface area, large pore volume, and defined pore size distribution.[1-5] Because of the possibility of tailoring the chemical and textural properties of carbonaceous matter numerous applications, such as gas/energy storage materials, supports of catalytic systems, adsorbents, and electrode materials, are feasible.[6] In previous work, we have reported several methods to synthesize microporous as well mesoporous carbon materials with different surface chemistry.[7] Corresponding materials are interesting candidates as cathode catalysts in polymer electrolyte membrane fuel cells (PEMFCs) because the research and development of non-noble metal catalysts for PEMFC is focused on highly porous carbon materials.[8-13]

Non-noble metal catalysts can be prepared by using different sources of carbon, nitrogen, and transition metals, such as iron and cobalt. Different approaches to prepare highly porous non-noble metal catalysts are reported in the literature.[14-16] For example, Medard et al. used transition metal-containing N_4 macrocycles, such as porphyrins and phthalocyanines, which have been adsorbed on activated carbon materials, and subsequently heat-treated in an inert atmosphere.[14] Matter et al. prepared oxygen reduction catalysts by chemical vapor deposition of acetonitrile over alumina-supported iron and nickel metal particles.[15] Bron et al. reported oxygen reduction catalysts prepared on the basis of heat-treated, carbon-supported iron phenanthroline complexes.[16]

Even though it is known that carbon, nitrogen, and transition metals are basic requirements for the formation of active catalysts, the structure of the active site in the corresponding catalysts is still a controversial issue in scientific literature. Dodelet proposed that heat-treatment of transition metal-containing N_4 macrocycles adsorbed on carbon supports results in active sites, which are supposed to be Co or Fe coordinated by four N atoms.[17] The nitrogen atoms are believed to be incorporated as pyridinic and pyrrolic-type structures in the carbon matrix. Other research groups suggest the catalytic formation of active sites in the presence of a transition metal, but the active site does not contain a metal atom at all.[18,19] Matter et al. suggested the role of the metal particles is likely that of a catalyst-forming active carbon-nitrogen nanostructures during pyrolysis.[15] The authors infer that the most active nanostructures contain nitrogen and have higher edge plane exposure, but the possibility that transition metals contribute to the catalytic activity cannot be excluded.

In the present study, we have investigated the catalytic activity toward oxygen reduction (ORR) of C–N–TM (TM-transition metal) materials, which have been prepared by a template-assisted synthesis route. The influence of the metal concentration in the template as well as the carbonization temperature toward the activity of the resulting catalyst materials has been studied. Furthermore, long-term stability testing regarding ORR activity has been carried out for selected catalyst samples.

Experimental

Sample preparation.— The catalyst samples were prepared by modification of the procedure described in Ref. 7. Briefly, a mesoporous silica gel (Koestrosorb 1015 donated by Chemiewerk Bad Koestritz, Germany) was treated with an aqueous solution of iron(III)-chloride or cobalt(II)-chloride. Different solutions with concentrations of 0.01, 0.1, and 0.2 M were used to impregnate the silica gel prior to loading with the carbon precursor, and 1 mL of metal salt solution was used to impregnate 1 g of silica gel. The mixtures were transferred into an oven, where they were dried at 80°C for 12 h. After drying, impregnated silica gel samples were loaded with pyrrole according to the remaining pore volume. The remaining pore volume was ~1 cm^3/g in all samples; thus, 1 mL pyrrole was used per gram of impregnated silica gel. In order to polymerize the polymer precursor, the pyrrole-loaded silica gel samples were exposed to HCl vapor. After complete polymerization, which was monitored by thermal analysis (see Fig. 1), all samples were carbonized. Final carbonization took place in a horizontal tube furnace, which was operated with argon gas. Each sample was heated at a rate of 2°C/min up to carbonization temperatures between 800 and 1100°C, and held for a subsequent dwell time of 2 h. To remove the template framework from the obtained silica/carbon composite material, 5–40% hydrofluoric acid was used. Composite materials were initially treated with 5% hydrofluoric acid for 1 h and additionally washed with 40% hydrofluoric acid to remove residual silica (and presumably some transition metal). The liberated catalyst materials were collected on filter paper, thoroughly washed with distilled water, and dried at 100°C afterward. For all prepared

* Electrochemical Society Active Member.
z E-mail: jeff.dahn@dal.ca

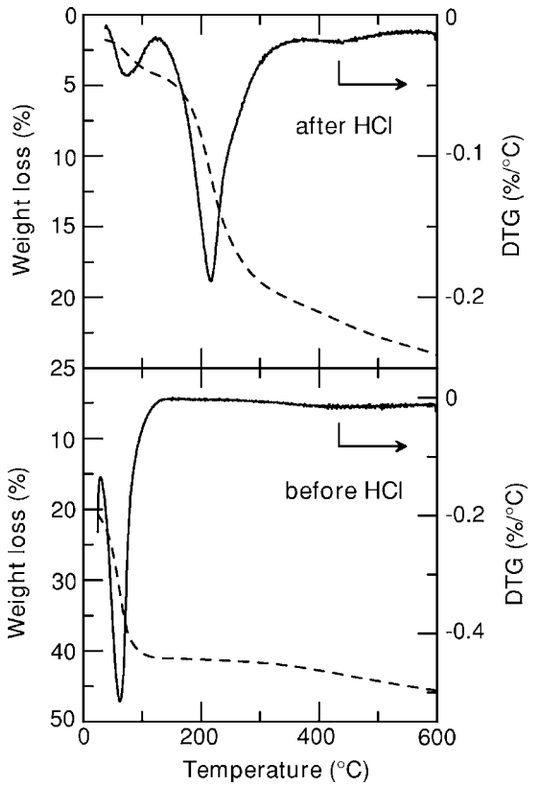

Figure 1. TGA curves (dashed line) and DTG curves (solid line) of the pyrrole-loaded silica gel samples of the resulting catalyst 0.1-Fe-800 before (bottom graph) and after HCl treatment (top graph). Measurements were done in argon atmosphere at a heating rate of 10°C/min.

samples, 0.8–1.2 g catalyst material was obtained from 5 mL pyrrole and 5 g of initial template. The targeted metal loading of the catalyst samples from the Fe- and Co-series with regard to the concentration of $FeCl_3$ and $CoCl_2$-solution used is given in Table I.

Nomenclature.— Catalyst sample 0.1-Fe-800 was prepared by using a 0.1 M $FeCl_3$ solution and a final carbonization at a temperature of 800°C in argon. In the case of sample 0.2-Co-900, a 0.2 M $CoCl_2$ solution was used for impregnation of the silica gel and heat-treatment was carried out at 900°C. All other samples are labeled in the same manner. SC stands for silica gel/carbon composite. The two carbon samples Suc-800 and Pyr-800 have been prepared by using the carbon precursors sucrose and pyrrole, respectively. Both samples were made by impregnating sucrose and pyrrole into mesoporous silica gel, which was not further impregnated with metal salt solution. Heat-treatment of the samples Suc-800 and Pyr-800 was carried out at 800°C.

Table I. Targeted metal loading of the catalyst samples from the Fe and Co series.

	Fe (wt %)	Co (wt %)	Solution used
0.01-Fe-800	0.35	—	0.01 M $FeCl_3$
0.1-Fe-800	3.5	—	0.1 M $FeCl_3$
0.2-Fe-800	7.0	—	0.2 M $FeCl_3$
0.01-Co-800	—	0.45	0.01 M $CoCl_2$
0.1-Co-800	—	4.5	0.1 M $CoCl_2$
0.2-Co-800	—	9.0	0.2 M $CoCl_2$

Characterization.— *Thermal analysis*.— In order to monitor the polymerization of pyrrole in the silica gel, the polymer/template composites were investigated by thermogravimetric analysis (TGA). The analysis was carried out using a thermal analysis (TA) instruments SDT Q600 thermobalance. All measurements were made in an argon atmosphere with a heating rate of 10°C/min. Experiments were started at room temperature and performed until a temperature of 600°C was reached.

Nitrogen adsorption.— Textural properties of the prepared catalyst samples were investigated using a Micromeritics ASAP 2000 analyzer. Nitrogen was used as adsorbate at −196°C. All catalyst samples were outgassed under vacuum overnight at 180°C. The surface area was calculated from the Brunauer, Emmett, and Teller method (BET) equation. The total pore volume was determined from the adsorbed nitrogen volume at a relative pressure of 0.95. Pore size distributions were calculated using density functional theory (DFT) for slitlike pore geometry. The DFT plus software used was provided by Micromeritics.

X-ray diffraction.— The crystal structures of the parent silica gel, silica gel/carbon composites and liberated catalyst samples were examined by means of X-ray diffraction (XRD) analysis. Corresponding measurements were carried out using a Siemens D5000 instrument with Cu Kα radiation (λ = 1.5418 Å). XRD patterns were recorded over a scattering angle range of 10–90° with 0.05° increments.

Scanning electron microscopy.— To observe the microscopic features of the silica gel, silica gel/carbon composites, and the resulting catalyst samples, high-resolution images were taken using a cold field emission Hitachi S-4700 scanning electron microscope (SEM). Imaging was carried out at 5 kV accelerating voltage by applying the secondary electron imaging technique.

Elemental analysis.— The composition of the prepared catalysts was investigated with a JEOL JXA-8200 superprobe electron microprobe system. The instrument consists of one energy dispersive spectrometer and five wavelength dispersive spectrometers. Fe, Co, C, N, O, and Si atomic compositions were all determined by wavelength dispersive spectroscopy (WDS) detectors. For the analysis of the catalyst samples, an accelerating voltage of 3 kV was chosen.

Electrochemical characterization.— The oxygen reduction behavior of the catalyst samples was investigated with the rotating ring-disk electrode (RRDE) technique. The electrochemical measurements were made using a Pine electrochemical instrument, which was equipped with an AFMSRX rotator and AFCBP1 bipotentiostat. The RRDE electrode was an assembly that consists of a catalyst film-coated glassy carbon (GC) disk (5 mm diam) held in a Teflon U-cup, which is surrounded by a Pt ring (7.5 mm i.d. and 8.5 mm o.d.). The GC disk was coated with 10 μL of a suspension of catalyst sample (10 mg) in a mixture of 350 μL ethanol and 95 μL 5% Nafion solution (Alfa Aesar). After the catalyst film was dried, electrochemical measurements were carried out.

The electrochemical measurements were performed in a one-compartment glass cell. Prior to the experiments the cell glassware was boiled in nanopure water (18 MΩ Barnstead) and rinsed with 0.1 M $HClO_4$ solution prepared from double-distilled $HClO_4$ (GFS Chemicals Inc.).

A Pt-wire counter electrode and a Hg/Hg_2SO_4 reference electrode were used for the measurement. A solution of 0.1 M $HClO_4$ was used as electrolyte. The potential calibration of the Hg/Hg_2SO_4 reference electrode was done vs the reversible hydrogen electrode (RHE). The potentials discussed in this publication have been corrected to the RHE potential. All measurements were carried out at ambient temperature.

The catalyst-coated GC disks were electrochemically cleaned by sweeping the potential between 0 and 1.0 V (vs RHE) at a sweep rate of 50 mV s^{-1} in an argon-saturated electrolyte solution until four consistent sweeps were obtained. A further cyclic voltammogram (CV) was collected in argon-purged 0.1 M $HClO_4$ solution from 1.0 to 0.05 V at a sweep rate of 5 mV s^{-1} to determine the non-faradaic current. For oxygen reduction reaction studies, oxygen

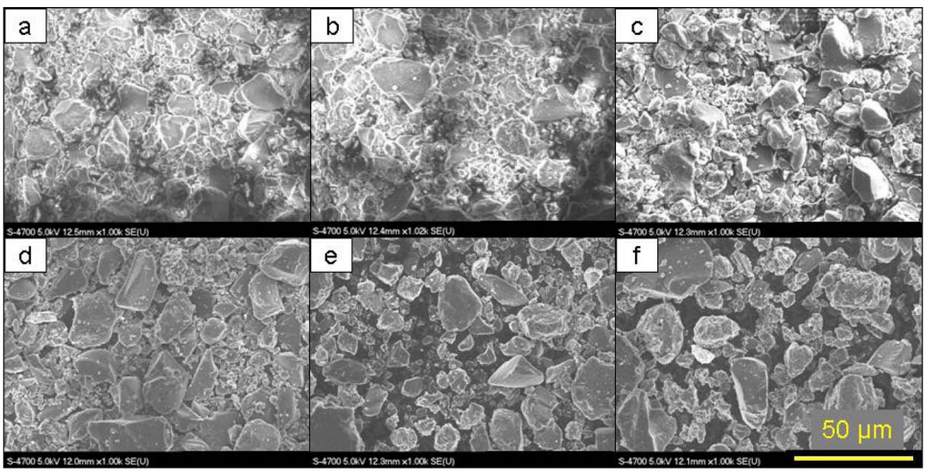

Figure 2. (Color online) SEM images of (a) silica gel and the liberated samples (b) Suc-800, (c) Pyr-800, (d) 0.01-Co-800, (e) 0.2-Co-800, and (f) 0.2-Fe-800.

was purged for 3 min through the cell and subsequent CVs were recorded while oxygen was still bubbling. Corresponding CVs were recorded from 1.0 to 0.05 V at 5 mV s^{-1}. The electrode was rotated at a rate of 900 rpm. The faradaic current was obtained by subtracting the CV in Ar-saturated electrolyte solution from that obtained in oxygen-saturated electrolyte solution.

In order to oxidize the H_2O_2 that was generated during the electrochemical experiments, the ring potential was held at 1.2 V vs RHE.[20] The $\%H_2O_2$ produced was calculated with[21]

$$\%H_2O_2 = 100\frac{2I_R/N}{I_D + (I_R/N)} \quad [1]$$

where I_D is the faradaic disk current, I_R is the faradaic ring current, and $N = 0.22$ is the RRDE collection efficiency. The collection efficiency of the ring electrode was calibrated as described in Ref. 21.

Results and Discussion

Thermal analysis.— The pyrrole-loaded silica gel samples of the resulting catalyst 0.1-Fe-800 were analyzed in order to monitor the polymerization as well as the carbonization of the carbon precursor. Therefore, the mass change of pyrrole-loaded silica gel samples at different stages was recorded during heat-treatment in an argon gas stream. One sample was treated with hydrochloric acid prior to the measurement, and the other sample was only loaded with pyrrole without further treatment. The obtained mass changes and corresponding derivative curves are given in Fig. 1. The weight loss of the untreated sample is given in the bottom graph, which shows a single step loss of 42% by mass.

The derivative reveals a maximum weight loss at a temperature of 62°C. This release is due to adsorbed pyrrole monomer, because the silica gel does not consist of strong adsorption sites or active sites to retain or polymerize pyrrole molecules, respectively. This also explains, that ~20% of the adsorbed pyrrole molecules have already been removed during the isothermal desorption in argon flow (20 min) prior to the heating ramp during analysis. Even though some transition metal ions such as Fe^{3+} catalyze the polymerization of pyrrole and corresponding derivates,[22] the amount of polypyrrole produced within the template pores was found to be negligible without HCl-treatment. Because 1 mL pyrrole was used per gram of impregnated silica gel and a final weight loss of ~46% by mass was observed after heating to 600°C, one can conclude that little to no carbon is left in the host material after heat-treatment. Furthermore, the residual material obtained after the thermal analysis experiment appeared to be a white-grayish powder.

The mass change and corresponding derivative of the pyrrole-loaded sample, which was treated with hydrochloric acid, are shown in the top graph of Fig. 1. The differential thermogram (DTG) curve shows a multistep loss of different components. An initial mass loss at around 66°C was still observed, but the weight change at this temperature was found to be only 4.4% by mass. This implies that polymerization of pyrrole occurred after HCl exposure. A second mass loss of 14.6% can be seen at 215°C. This weight change presumably results from the depolymerization and decomposition of polypyrrole encapsulated in the template material.[23] A total weight loss of 24% by mass was determined after heating to 600°C. After the thermal analysis of the HCl-treated sample, a black powder was recovered from the heating pan of the SDT Q600 thermobalance. By comparing the thermal analysis data of both samples, it can be concluded that the carbon precursor was only partially removed from the host material in the case of the HCl-treated sample, whereas all carbon precursor was removed from the untreated template sample. Hence, the HCl-treatment is a crucial step during synthesis in order to achieve complete bulk polymerization of pyrrole, which will give sufficient carbon material located in the interconnected pore network of the template material. All materials prepared during this study have been investigated by means of thermal analysis. No difference was observed for the different pyrrole-loaded silica gel samples with regard to varying $FeCl_3$ or $CoCl_2$ contents.

Scanning electron microscopy.— Scanning electron microscopy images were taken of the liberated carbon and catalyst samples, silica gel/carbon composites, and the parent silica gel template. Corresponding images of the template and the carbon materials Pyr-800 and Suc-800 are given in Fig. 2a-c. The SEM images reveal that the carbon material made of pyrrole, Pyr-800 (Fig. 2c), has the same particle size and shape as the inorganic template (Fig. 2a) and the silica gel/carbon composite (not shown). These results indicate a successful template-assisted synthesis. No differences were observed for another carbon sample, Suc-800 (Fig. 2b), which was prepared using a different carbon precursor, sucrose.[24] The SEM images are similar to previously prepared carbon replicas described by Ma et al.[25] and Garsuch and Klepel.[26] SEM shows a broad particle size distribution of the samples prepared in this study. The particle diameters range from 20 nm to > 10 µm. SEM images of the catalyst samples 0.01-Co-800, 0.2-Co-800, and 0.2-Fe-800 are shown in Fig. 2d-f. The morphology of the prepared catalyst samples is the same as that observed for the carbon-nitrogen materials without metal source.

Nitrogen adsorption experiments.— The textural properties of prepared catalyst samples were investigated by means of nitrogen adsorption experiments at −196°C. Nitrogen adsorption isotherms of samples prepared with different metal sources ($FeCl_3$, $CoCl_2$), and varying metal loadings are displayed in the left graphs of Fig. 3. The samples were carbonized at 800°C. The determined BET surface areas, micropore areas, and total pore volumes of all investigated catalyst samples are summarized in Table II.

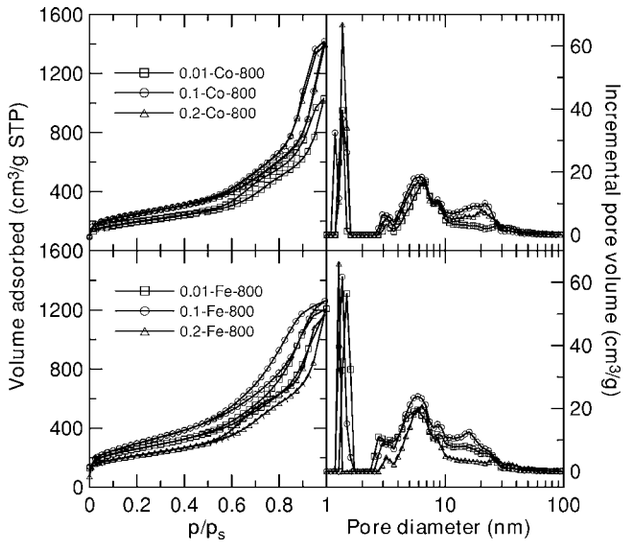

Figure 3. Nitrogen adsorption/desorption isotherms and pore size distributions of the prepared catalyst samples from Fe- (bottom graphs) and Co-series (top graphs). Corresponding catalysts were carbonized at 800°C.

The nitrogen adsorption isotherms of all prepared catalyst samples correspond to type-IV isotherms according to the classification of International Union of Pure and Applied Chemistry (IUPAC). The textural properties of the inorganic template have been investigated earlier and are given elsewhere in the literature.[24] The used silica gel also exhibits a type-IV isotherm, which is the characteristic feature of a mesoporous material. Prepared catalyst samples show pronounced capillary condensation steps, which start at relative pressure of 0.6 and occur over a wide relative pressure range up to $p/p_s = 1.0$ due to broad pore size distributions. The investigated samples possess mesoporosity in addition to microporosity. These results further confirm that the textural properties of the parent template material could be inherited by the prepared catalyst materials. BET surface areas between 740 m^2/g (0.2-Fe-800) and 1030 m^2/g (0.1-Fe-800) were determined in the case of catalysts made with $FeCl_3$. Total pore volumes varied from 1.9 to 2.4 cm^3/g. Catalyst samples prepared by using $CoCl_2$ exhibit BET surface areas ranging from 670 m^2/g (0.01-Co-800) to 850 m^2/g (0.2-Co-800). Corresponding samples have total pore volumes between 1.6 and 2.2 cm^3/g.

The micropore areas of the catalyst samples made with iron and cobalt varied between 63 and 138 m^2/g as shown in Table II. The majority of the catalyst samples exhibit a micropore area near 120 m^2/g. There was no significant change in the micropore area observed with regard to the metal source used or the metal concentration present within the host material. The samples Pyr-800 and Suc-800 showed similar textural properties, even though the determined values of surface area and total pore volume are somewhat higher.

Table II. BET surface area and total pore volume of prepared catalyst samples determined by nitrogen adsorption experiments.

	BET surface area ($m^2\ g^{-1}$)	Micropore area ($m^2\ g^{-1}$)	Total pore volume ($cm^3\ g^{-1}$)
0.01-Fe-800	910	120	1.9
0.1-Fe-800	1030	126	2.4
0.2-Fe-800	740	116	1.8
0.01-Co-800	670	63	1.6
0.1-Co-800	810	138	2.1
0.2-Co-800	850	121	2.2
Pyr-800	1200	—[a]	2.0
Suc-800	1350	—[a]	2.6

[a] Not determined.

Table III. Elemental composition of prepared catalyst samples determined by WDS[a].

	Fe (wt %)	Co (wt %)	C (wt %)	N (wt %)	O (wt %)
0.01-Fe-800	0.5	—[b]	86.1	7.6	5.8
0.01-Fe-800	2.0	—[b]	86.7	7.2	4.1
0.2-Fe-800	1.8	—[b]	88.8	7.7	1.7
0.01-Co-800	—[b]	0.5	88.8	9.2	1.4
0.1-Co-800	—[b]	1.4	86.5	10.4	1.7
0.2-Co-800	—[b]	1.4	87.0	9.5	2.1
Pyr-800	—[b]	—[b]	92.1	6.1	1.8
Suc-800	—[b]	—[b]	98.0	—[b]	2.0

[a] The accuracy in these measurements is about ±0.5 wt % for the measurements reported here.
[b] Elements were assumed to be absent and were not analyzed.

The estimated pore size distributions (PSD) of prepared samples are illustrated in the graphs on the right-hand side of Fig. 3. PSDs show that different pore sizes exist in the catalyst samples. Micropores with diameters <2 nm are present, which can be formed during the carbonization process beside the porosity generated through template removal. We have earlier suggested that the emission of small molecules such as water or carbon dioxide, causes the generation of an additional microporosity in the case of carbon replicas.[4] The PSDs also indicate the existence of mesoporosity. Mesopore diameters between 3 and 30 nm have been determined for the investigated samples. The mesoporosity was mainly generated due to the dissolution of the inorganic framework with hydrofluoric acid. Present results are in good agreement with earlier studies on carbon materials made by a template-assisted synthesis route.[27] There were no significant differences found in the obtained PSDs with regard to the metal source used. Nitrogen adsorption experiments clearly show that catalyst samples with a very high degree of porosity have been prepared. To the our best knowledge, only a few oxygen reduction catalysts possessing such high surface areas and pore volumes have been reported.[14,15]

Elemental composition.— The elemental composition of each catalyst was determined from the results of WDS measurements. The summarized data of WDS measurements of all catalyst samples prepared at 800°C are given in Table III. All prepared catalysts consist of carbon, oxygen, and nitrogen when pyrrole was used as the carbon precursor. The content of residual silicon was found to be <0.1 wt %, indicating complete removal of the inorganic template framework after treatment with hydrofluoric acid.

In general, carbon contents between 86.1 and 88.8 wt % were observed in the liberated catalysts samples, which are in agreement with previously performed X-ray photoelectron spectroscopy (XPS) experiments and elemental analysis of carbon replicas made from pyrrole and silica gel.[7] Oxygen fractions were found to vary between 1.4 and 5.8 wt %. The nitrogen contents ranged from 7.2 to 10.4 wt % in the case of the prepared non-noble metal catalyst samples. Former XPS studies on metal-free carbon replicas revealed the existence of pyridine-like nitrogen species as well as pyrrolic and pyrridinic-like nitrogen species.[7]

The total metal content in the prepared non-noble metal catalysts varied only between 0.5 and 2.0 wt %. The samples made by using $FeCl_3$ showed a maximum Fe-content of 2.0 wt %, and the samples prepared with $CoCl_2$-containing silica gel exhibit not more than 1.4 wt % Co. These results clearly show that the majority of each metal (Fe, Co) or metal compound ($FeCl_3$ or $CoCl_2$) has been leached out of the composite material during the treatment with

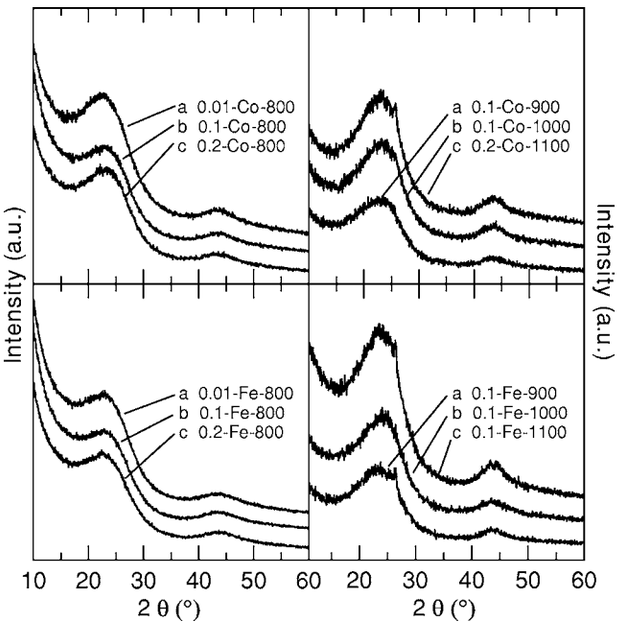

Figure 4. XRD measurements showing intensity vs scattering angle for prepared catalyst samples from Fe- (bottom graphs) and Co-series (top graphs). The XRD patterns on the left-hand side correspond to the catalyst samples carbonized at 800°C. XRD patterns on the right-hand side belong to the samples heat-treated between 900 and 1100°C.

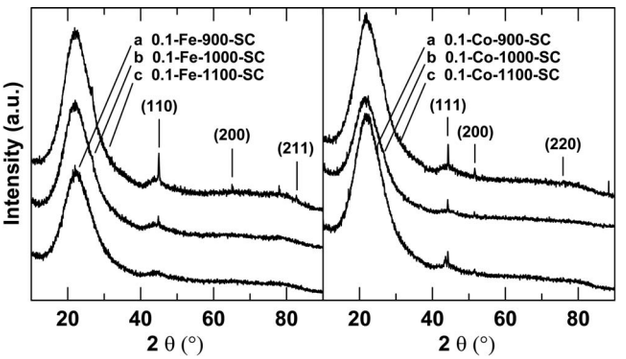

Figure 5. XRD measurements showing intensity vs scattering angle for the silica gel/carbon composite materials containing iron (left graph) and cobalt (right graph). The XRD patterns correspond to the silica gel/carbon composite materials heat-treated between 900 and 1100°C. The major Bragg peaks of the phases present are indicated.

hydrofluoric acid. The resulting catalyst samples do not retain the full metal loading of the corresponding composite materials, i.e., the targeted metal loading of the catalyst samples (see Table I and III). However, the determined metal fractions of the catalyst samples do not correlate with the initial concentration of $FeCl_3$ or $CoCl_2$ deposited as metal sources within the pores of the silica gel. For example, the amount of iron deposited in silica gel in order to prepare sample 0.2-Fe-800 is larger by a factor of 20 in comparison to sample 0.01-Fe-800. But the resulting catalyst samples do not show such a difference in their metal loadings. Hence, we assume that the leaching step with hydrofluoric acid results in the removal of metal source to a different extent in each case. The observed metal fractions are comparable to non-noble metal catalysts reported by Maruyama and Abe who have investigated highly porous carbons made by carbonization of hemoglobin.[28] Also Bron et al. reported that metal loadings ~1 wt % are present in highly active oxygen reduction catalysts made of heat-treated iron phenanthroline complexes supported on high surface area carbon blacks.[29]

XRD analysis.— The recorded XRD patterns of all liberated catalysts samples and the composite materials 0.1-Fe-900-SC, 0.1-Fe-1000-SC, 0.1-Fe-1100-SC, and 0.1-Co-900-SC, 0.1-Co-1000-SC, 0.1-Co-1100-SC are shown in Fig. 4 and 5. The abbrevation SC stands for silica gel/carbon composite. In the case of the catalyst samples (Fe-series and Co-series), broad peaks at an angle of $2\theta = 25°$ were observed. Smaller humplike peaks were observed at ~44°. These peaks can be attributed to amorphous carbon materials, such as carbon replicas, as well as activated carbon materials, which exhibit similar XRD patterns.[30-32] The peaks are due to the reflections from the (002) and (100) planes, revealing the turbostratic structure of the catalyst samples, which results from the low crystalline ordering of the carbon matrix. These characteristic features were also observed in case of the catalyst samples heat-treated at 900, 1000, and 1100°C. The increasing carbonization temperature had little effect on the crystalline ordering of the resulting catalysts.

XRD patterns of the composite materials 0.1-Fe-1000-SC and 0.1-Fe-1100-SC exhibit a sharp diffraction peak at $2\theta = 44.8°$. Catalyst sample 0.1-Fe-1100-SC also shows two additional peaks at $2\theta = 65.1$ and 82.4°. One can see that the peak intensities grow with an increase in the heat-treatment temperature. By comparing the XRD pattern of 0.1-Fe-1100-SC with the JCPDS database, the most probable match found was the X-ray pattern of α-Fe. The diffraction peaks observed at 44.8, 65.1, and 82.4° are assigned to the (110), (200), and (211) planes, respectively.

The XRD patterns of the silica gel/carbon composites 0.1-Co-900-SC, 0.1-Co-1000-SC, and 0.1-Co-1100-SC show a characteristic diffraction peak at $2\theta = 44.3°$, which is assigned to the (111) plane of β-Co.[33] Further diffraction peaks at 51.6 and 76.0° have been observed in the case of these sample. These peaks are attributed to the (200) and (220) planes of β-Co. These findings are in agreement with earlier work of Faubert et al., who could detect α-Fe and β-Co phases in heat-treated iron and cobalt tetraphenylporphyrins adsorbed on carbon black.[33]

The fact that iron and cobalt species can be detected in the silica gel/carbon-composites (Fig. 5) by means of XRD but not in the resulting catalyst samples (Fig. 4) further confirms that the majority of the metal source is leached out after treatment with hydrofluoric acid. Hence, XRD measurements confirm the results of electron microprobe measurements.

Electrochemical characterization.— All oxygen reduction catalysts obtained from the template-assisted synthesis procedure have been investigated using RRDE experiments. Electrocatalytic activity of each catalyst was determined from cyclic voltammetry measurements in 0.1 M $HClO_4$ solution saturated with oxygen at room temperature. All RRDE data shown in this study were collected with the electrode rotating at 900 rpm. For comparison purposes, the data obtained for a sputtered Pt film on a GC disk is given in each graph.

The cathodic scan of each cyclic voltammogram of the catalyst samples from the Fe- and Co-series recorded during oxygen reduction reaction are given in Fig. 6 (left graphs). The hydrogen peroxide production calculated from the observed ring currents is also shown in Fig. 6 (right graphs). Figure 6 demonstrates that all prepared catalyst samples heat-treated at 800°C show obvious electrocatalytic activity toward oxygen reduction. Increasing metal contents in the silica gel samples significantly increase the catalytic activity of the resulting non-noble metal catalysts, as shown in the depicted graphs. Sample 0.01-Co-800 exhibits an onset potential at 0.72 V, whereas the catalyst samples 0.1-Co-800 and 0.2-Co-800 show onset potentials at values of 0.83 and 0.81 V, respectively. In the case of sample 0.01-Fe-800, an onset potential of 0.81 V is observed. The catalyst samples 0.1-Fe-800 and 0.2-Fe-800 prepared with silica gel having higher metal loadings show onset potentials between 0.85 and 0.83 V, respectively. Higher current densities are observed in the case of Fe-containing catalysts. The results indicate that better catalyst samples are generated in the presence of iron, which is also in

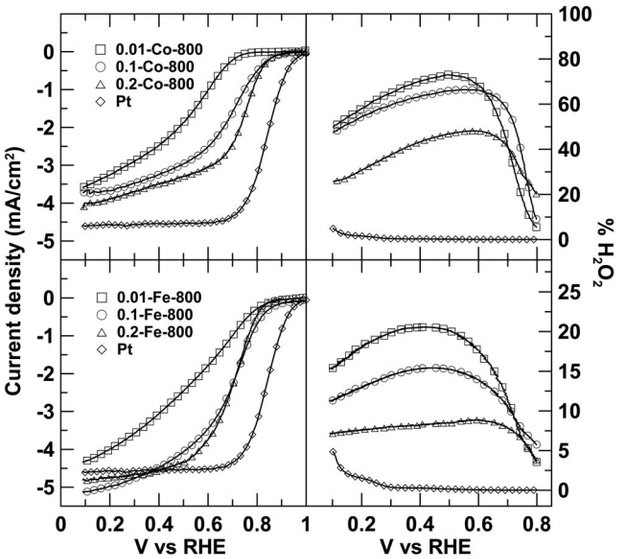

Figure 6. Left-hand side: disk current densities for catalyst samples from Fe-series (bottom graphs) and Co-series (top graphs) carbonized at 800°C, and sputtered Pt film on GC disks. Right-hand side: $\%H_2O_2$ produced as a function of disk potential for corresponding samples. Measurements were carried out in O_2-saturated 0.1 M $HClO_4$ at 25°C. The sweep rate is 5 mV s^{-1}, and the rotation speed is 900 rpm.

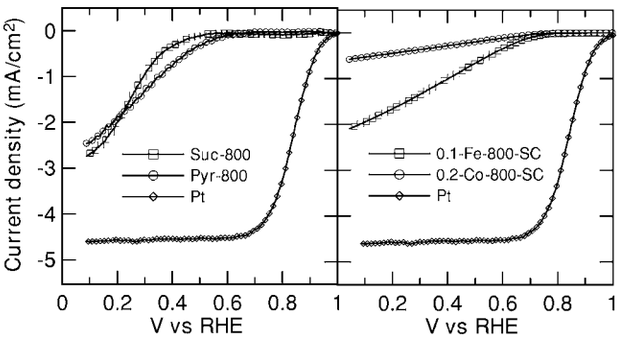

Figure 7. Disk current densities for catalyst samples Suc-800, Pyr-800, and sputtered Pt film on GC disk (left-hand side) and silica gel/carbon composite materials 0.1-Fe-800, 0.2-Co-800, and sputtered Pt film on GC disk (right-hand side). Measurements were carried out in O_2-saturated 0.1 M $HClO_4$ at 25°C. The sweep rate is 5 mV s^{-1}, and the rotation speed is 900 rpm.

agreement with the calculated percentage of hydrogen peroxide produced during oxygen reduction. The graphs showing hydrogen peroxide production reveal that increasing metal content in the silica gel samples significantly reduce the amount of hydrogen peroxide produced by the resulting catalyst samples. In the case of samples from the Co-series, hydrogen peroxide production between 48 and 73% is observed. Corresponding catalysts from the Fe-series give values ranging from 8 to 20%, which is similar to the values of iron-containing catalysts reported by Bron et al.[29] The considerable difference in hydrogen peroxide production between the Fe and Co catalyst series cannot yet be clarified and requires further investigation.

Even though the catalytic activity of the prepared catalysts increase when more metal source is present in the silica gel pores, it does not correlate with the metal loading of the final catalysts. Elemental analysis revealed that metal fractions varied between 0.5 and 2.0 wt % only. The results show that the transition metals are involved in the active site formation, but according to the present results and, in our opinion, the scientific literature, it is not possible to say at this point whether the metal is involved in the active site or not. The template-assisted synthesis route generates active sites, as demonstrated by the catalytic activity of our prepared catalyst samples.

In order to check if the presence of iron or cobalt is also required for our nanocasted catalyst samples, oxygen reduction experiments on samples made without metal source have been carried out. The cathodic scans of the collected CVs for the sample Pyr-800 and Suc-800 are shown in Fig. 7 (left-hand side). The lower onset potential with a value of 0.39 V is observed for sample Suc-800, which was prepared by using a non-nitrogen containing carbon precursor, sucrose. A higher onset potential of 0.54 V was found in the case of nitrogen-containing sample Pyr-800. The observed onset potentials and current densities are significantly lower in comparison to metal-containing catalysts. These findings confirm that a metal source is also required for the formation of active sites in catalyst samples prepared via a template-assisted synthesis route. Nevertheless, present results demonstrate that the nitrogen-containing carbon material Pyr-800 is more active for the oxygen reduction reaction than the carbon material Suc-800.

In addition, the silica gel/carbon composite materials 0.1-Fe-800-SC and 0.2-Co-800-SC have been analyzed with regard to their catalytic activity toward oxygen reduction. The cathodic scans of the recorded CVs are given in Fig. 7 (right-hand side). The composite samples show onset potential values of 0.71 V (0.1-Fe-800-SC) and 0.73 V (0.2-Co-800-SC). Only low current densities were observed for the composite materials. The obtained results prove that catalytically active material is present in the composite samples, but the composites also contain nonactive silica gel. Because 10 mg of sample is used to prepare the catalyst coating of the GC disk, the silica part of the composites "dilutes" the number of active sites. Hence, the leaching step with hydrofluoric acid cannot be omitted in order to achieve high catalytic activity.

Further catalyst samples were prepared to investigate the effect of carbonization temperature toward the oxygen reduction reaction. These catalyst samples were prepared by using a silica gel impregnated with 0.1 M $FeCl_3$ or 0.1 M $CoCl_2$ solution. The final carbonization temperatures ranged from 900 to 1100°C. The results of the RRDE experiments are given in Fig. 8. The cathodic scans of the collected CVs are shown in the graphs on the left-hand side, whereas the calculated hydrogen peroxide production is given in the graphs on the right-hand side. For the Fe-containing samples 0.1-Fe-800, 0.1-Fe-900, and 0.1-Fe-1000, recorded cathodic scans of the CVs obtained under oxygen are on top of each other. This shows that the catalytic activity of the catalyst material has not significantly changed in this particular temperature range. Recent studies of Gadiou et al. have revealed that carbon materials prepared by a template-assisted synthesis route display characteristics (structure, graphitization degree), which are different from carbon materials made by direct carbonization of the precursors.[34] The authors suggest a relation between the different characteristics and the fact that the synthesis of the corresponding materials takes place in a confined space. The carbonization within an interconnected three-dimensional network having pore size between 1 and 13 nm (silica gel) may result in different graphitization behavior because the orientation of the graphene layers depends on the geometry of the template where carbonization takes place.[34] Hence, we assume that a temperature increase of 200°C has no considerable impact on the composition as well as the structure of the prepared catalyst material, which agrees well with the results from XRD measurements. The heat-treated sample 0.1-Fe-1100 exhibits an onset potential at 0.77 V, which is significantly lower than the onset potential (0.85 V) of the other samples. The hydrogen peroxide production is about the same in case of the samples 0.1-Fe-800, 0.1-Fe-900, and 0.1-Fe-1000 (12–15%), whereas a value of 37% was calculated for sample 0.1-Fe-1100.

Similar results were observed for the samples from the Co-series. The onset potential was reduced from 0.83 V (0.1-Co-800) to

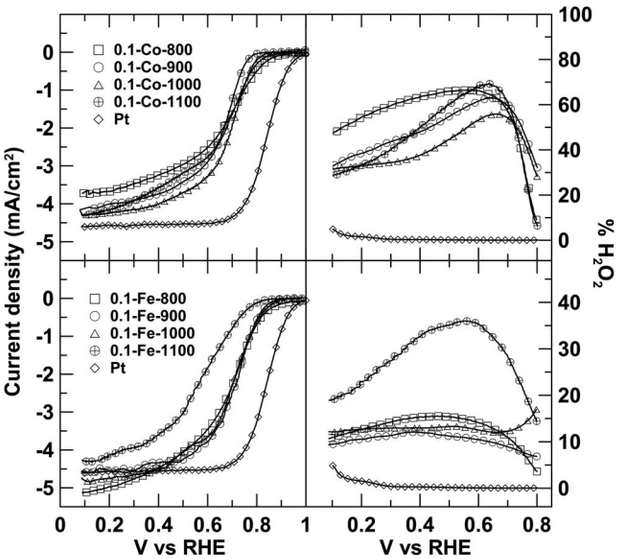

Figure 8. Disk current densities (left-hand side) for catalyst samples from Fe-series (bottom graphs) and Co-series (top graphs), heat-treated between 800 and 1100°C, and sputtered Pt film on GC disk. $\%H_2O_2$ produced (right-hand side) as a function of disk potential for corresponding samples. Measurements were carried out in O_2-saturated 0.1 M $HClO_4$ at 25°C. The sweep rate is 5 mV s^{-1}, and the rotation speed is 900 rpm.

0.76 V in case of the catalyst 0.1-Co-1100, which was heat-treated at the highest carbonization temperature in this study. The difference in hydrogen peroxide production was not that significant because the values were already above 50%. The values of peroxide production range from 56 to 70% in the case of the Co-containing catalysts. It is clear that heat-treatment above 1000°C results in decreasing catalytic activity of the prepared non-noble metal catalysts. These findings are in agreement with the earlier work of Easton et al., who have investigated sputtered Fe–C–N and Co–C–N films.[35] The authors report a decreasing catalytic activity at higher annealing temperatures. Easton et al. mentioned that a maximum activity was achieved at 800°C and it decreased upon heating the catalyst films to 1000°C.[35] The authors suspect that the loss of nitrogen during heating at higher temperature is responsible for the reduced catalytic activity.

Stability measurements were also carried out on selected catalyst samples 0.1-Fe-900, 0.1-Fe-1000, 0.1-Co-900, and 0.1-Co-1000. During the experiments, disk currents were recorded while the potential was held at 0.6 V. The obtained current densities vs time are depicted in Fig. 9. The results show good long-term stability because catalytic activity decays slightly for all investigated samples within 16 h. Catalyst samples prepared with $FeCl_3$-containing silica gel exhibit higher current densities as mentioned above. For samples 0.1-Fe-900 and 0.1-Fe-1000, the current density was reduced to 88.6 and 86% of the initial value after 16 h. Samples 0.1-Co-900 and 0.1-Co-1000 showed current density values of 94 and 91% of the start point after the same time period. Catalyst samples 0.1-Co-1000 and 0.1-Fe-900 have been tested for further 94 and 44 h, respectively. In case of sample 0.1-Co-1000, the obtained current density was still 79% of the initial value after 110 h. Sample 0.1-Fe-900 exhibited a current density value of 83% after 60 h. However, the potential hold experiment of sample 0.1-Fe-900 was stopped after the Teflon U-cup of the electrode assembly started to leak. Both samples show the same trend for the first 60 h, indicating a similar degradation process. Nevertheless, the long-term measurements prove high catalytic activity and durability of the prepared catalyst samples made by the template-assisted synthesis route.

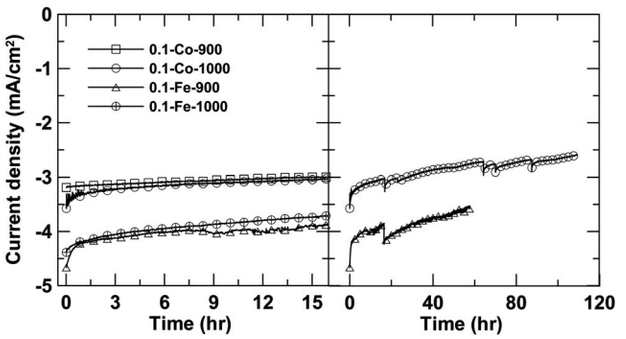

Figure 9. Current density plotted vs time for the catalyst samples 0.1-Fe-900, 0.1-Fe-1000, 0.1-Co-900, and 0.1-Co-1000. Measurements were carried out in O_2-saturated 0.1 M $HClO_4$ at 25°C. The potential was held at 0.6 V, and the rotation speed is 900 rpm.

Conclusion

In the present study, a new synthesis route for the preparation of non-noble metal catalysts has been reported. A template-assisted synthesis route was applied in order to generate catalyst materials having high surface area as well as high degree of porosity by using silica gel as a template and pyrrole as a carbon precursor. $FeCl_3$ and $CoCl_2$ have been used as metal sources. Obtained catalyst samples possess BET surface areas between 670 and 1030 m^2/g and pore volumes ranging from 1.6 to 2.4 cm^3/g. Electron microprobe and XRD measurements revealed that much of the metal source is leached out after treatment with hydrofluoric acid. All prepared catalyst samples heat-treated between 800 and 1100°C show electrocatalytic activity toward oxygen reduction. Onset potentials up to 0.85 V and hydrogen peroxide production below 10% were observed during the oxygen reduction reaction for the best catalyst samples. The obtained catalysts show high catalytic activity and good long-term stability. Therefore, we assume that a high number of active sites are generated by the template-assisted synthesis route. This synthesis route results in a distorted structure of graphite layers having nitrogen as well as higher edge plane exposure. We assume that the open structure and high surface area of these catalyst materials give rise to the high catalytic activity. It has been demonstrated that the type of metal source, metal concentration within host material, and carbonization temperature have an impact on the catalytic activity toward oxygen reduction.

Acknowledgments

We thank S. Wang for performing the SEM measurements and P. Stoffyn-Egli for help in obtaining electron microprobe data. Special thanks to D. Stevens and T. Byrne for helpful discussions.

Dalhousie University assisted in meeting the publication costs of this article.

References

1. T. Kyotani, T. Nagai, S. Inoue, and A. Tomita, *Chem. Mater.*, **9**, 609 (1997).
2. S. A. Johnson, E. S. Brigham, P. J. Ollivier, and T. E. Mallouk, *Chem. Mater.*, **9**, 2448 (1997).
3. R. Ryoo, S. H. Joo, and S. Jun, *J. Phys. Chem. B*, **103**, 7743 (1999).
4. A. Garsuch, W. Böhlmann, R. R. Sattler, J. Fraissard, and O. Klepel, *Carbon*, **44**, 1173 (2006).
5. C. J. Meyers, S. D. Shah, S. C. Patel, R. M. Sneeringer, C. A. Bessel, N. R. Dollahon, R. A. Leising, and E. S. Takeuchi, *J. Phys. Chem. B*, **105**, 2143 (2001).
6. F. Su, J. Zeng, Y. Yu, L. Lv, J. Y. Lee, and X. S. Zhao, *Carbon*, **43**, 2366 (2005).
7. A. Garsuch, R. R. Sattler, S. Witt, and O. Klepel, *Microporous Mesoporous Mater.*, **89**, 164 (2006).
8. G. Lalande, R. Cote, G. Tamizhmani, D. Guay, J. P. Dodelet, L. Dignard-Bailey, L. T. Weng, and P. Bertrand, *Electrochim. Acta*, **40**, 2635 (1995).
9. A. H. C. Sirk, S. A. Campbell, and V. I. Birss, *Electrochem. Solid-State Lett.*, **8**, A104 (2005).
10. K. Sawai and N. Suzuki, *J. Electrochem. Soc.*, **151**, A2132 (2004).
11. M. Bron, S. Fiechter, P. Bogdanoff, and H. Tributsch, *Fuel Cells*, **2**, 137 (2002).
12. S. Lj. Gojkovic, S. Gupta, and R. F. Savinell, *J. Electrochem. Soc.*, **145**, 3493

(1998).
13. G. Q. Sun, J. T. Wang, S. Gupta, and R. F. Savinell, *J. Appl. Electrochem.*, **31**, 1025 (2001).
14. C. Medard, M. Lefevre, J. P. Dodelet, F. Jaouen, and G. Lindbergh, *Electrochim. Acta*, **51**, 3202 (2006).
15. P. H. Matter, E. Wang, M. Arias, E. J. Biddinger, and U. S. Ozkan, *J. Phys. Chem. B*, **110**, 18374 (2006).
16. M. Bron, J. Radnik, M. Fieber-Erdmann, P. Bogdanoff, and S. Fiechter, *J. Electroanal. Chem.*, **535**, 113 (2002).
17. J. P. Dodelet, in *N_4 Macrocyclic Metal Complexes*, J. H. Zagal, F. Bedioui, and J. P. Dodelet, Editors, p. 83, Springer, New York (2006).
18. P. Gouerec, A. Biloul, O. Contamin, G. Scarbeck, M. Savy, J. Riga, L. T. Weng, and P. Bertrand, *J. Electroanal. Chem.*, **442**, 61 (1997).
19. S. Lj. Gojkovic, S. Gupta, and R. F. Savinell, *J. Electroanal. Chem.*, **462**, 63 (1999).
20. O. Antoine and R. Durand, *J. Appl. Electrochem.*, **30**, 839 (2000).
21. U. A. Paulus, T. J. Schmidt, H. A. Gasteiger, and R. J. Behm, *J. Electroanal. Chem.*, **495**, 134 (2001).
22. A. Garsuch, R. R. Sattler, and P. G. Pickup, *Chem. Commun. (Cambridge)*, **3**, 344 (2004).
23. A. Garsuch, Ph.D. Thesis, University of Leipzig (2006).
24. K. Böhme, W.-D. Einicke, and O. Klepel, *Carbon*, **43**, 1918 (2005).
25. Z. Ma, T. Kyotani, and A. Tomita, *Carbon*, **40**, 2367 (2002).
26. A. Garsuch and O. Klepel, *Carbon*, **43**, 2330 (2005).
27. O. Klepel, A. Garsuch, and K. Böhme, *Stud. Surf. Sci. Catal.*, **158A**, 469 (2005).
28. J. Maruyama and I. Abe, *Chem. Mater.*, **18**, 1303 (2006).
29. M. Bron, S. Fiechter, M. Hilgendorff, and P. Bogdanoff, *J. Appl. Electrochem.*, **32**, 211 (2002).
30. P. M. Barata-Rodrigues, T. J. Mays, and G. D. Moggridge, *Carbon*, **41**, 2231 (2003).
31. S. Blazewicz, A. Swiatkowski, and B. J. Trznadel, *Carbon*, **37**, 693 (1999).
32. P. J. M. Carrott, J. M. V. Nabais, M. M. L. Ribeiro Carrott, and J. A. Pajares, *Carbon*, **39**, 1543 (2001).
33. G. Faubert, G. Lalande, R. Cote, D. Guay, J. P. Dodelet, L. T. Weng, P. Bertrand, and G. Denes, *Electrochim. Acta*, **41**, 1689 (1996).
34. R. Gadiou, A. Didion, S. E. Saadallah, M. Couzi, J. N. Rouzaud, P. Delhaes, and C. Vix-Guterl, *Carbon*, **44**, 3348 (2006).
35. E. B. Easton, R. Yang, A. Bonakdarpour, and J. R. Dahn, *Electrochem. Solid-State Lett.*, **10**, B6 (2007).